Supporting Information for

Rapid Newcastle Disease Virus Detection based on Loop-Mediated Isothermal Amplification and Optomagnetic Readout

Bo Tian,[†] Jing Ma,[‡] Teresa Zardán Gómez de la Torre,[†] Ádám Bálint,[#] Marco Donolato,[§] Mikkel Fougt Hansen,[‖] Peter Svedlindh,[†] and Mattias Strömberg*[,†]

[†] Department of Engineering Sciences, Uppsala University, The Ångström Laboratory, Box 534, SE-751 21 Uppsala, Sweden

[‡] Department of Immunology, Genetics and Pathology, Uppsala University, The Rudbeck Laboratory, SE-751 85 Uppsala, Sweden

[#] National Food Chain Safety Office, Veterinary Diagnostic Directorate, Tábornok u. 2., H-1143 Budapest, Hungary

[§] BluSense Diagnostics, Fruebjergvej 3, 2100 Copenhagen, Denmark

[‖] Department of Micro- and Nanotechnology, Technical University of Denmark, DTU Nanotech, Building 345 East, DK-2800 Kongens Lyngby, Denmark

Table of Contents

S1. Optomagnetic system description and optomagnetic measurement principle.

As illustrated in **Fig. S1**, the set-up employed for optomagnetic effect measurement was based on an unfocused 405 nm laser source (Sony optical unit, Sony, JP) and a photodetector (PDA36A, Thorlabs Inc., U.S.A.). Powered by a software controlled current source, the laser source provided a linearly polarized light beam (diameter of 2 mm), and the polarization direction was oriented along the axis of the applied magnetic field. A disposable UV-transparent cuvette (REF 67.758.001, SARSTEDT, Nümbrecht, Germany) was positioned in the beam path, centred between a pair of electromagnets (1433428C, Murata Power Solutions Inc., U.S.A.). The optical path through the liquid in the cuvette was 10 mm. The distance between the electromagnets was 20 mm, and the distance between laser source and detector was 115 mm. The LabVIEW controlled electromagnets were powered by an AC source. The AC magnetic field was applied perpendicular to the laser beam, and the maximum AC magnetic field amplitude was limited to approximately 2.6 mT in the current set-up. The self-inductance of the electromagnets was corrected for to ensure constant field amplitude and phase at all frequencies. The laser, electromagnets, cuvette, and detector were covered during measurements to avoid interference from external light sources. The detector signal was converted from analogue to digital by a data acquisition unit (DAQ unit, NI USB-6341, National Instruments, U.S.A.), followed by further processing in the computer by a FFT enabled lock-in function.

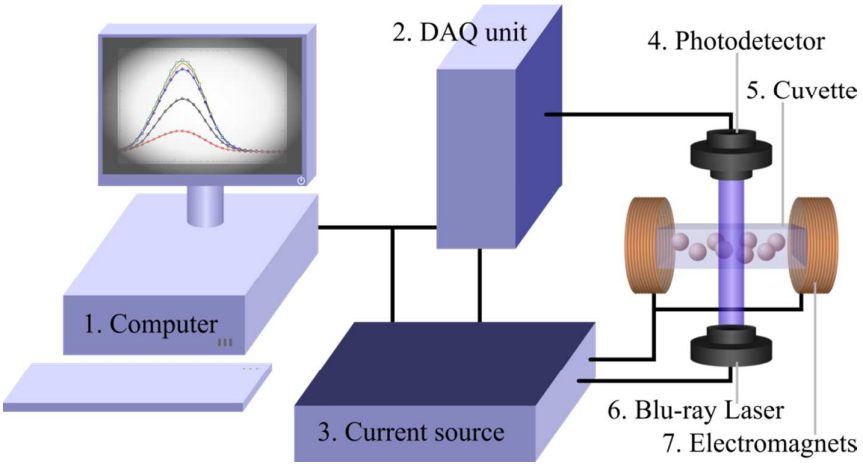

Figure S1. Schematic illustration of the optomagnetic set-up. The liquid sample, contained in an optically transparent cuvette (5), is placed between two identical electromagnets (7). A 405 nm laser source (6) generates a laser beam aimed at the bottom of the cuvette. The transmitted light detected by a photo detector (4) is recorded *vs.* time using a DAQ unit (2). The laser and electromagnets are powered by a current source (3). A computer (1) controls the entire set-up and performs the software based lock-in detection.

The optomagnetic measurement principle is based on the rotational dynamics of magnetic nanoparticles (MNPs). The MNPs employed in this study have a remanent magnetic moment, which implies that the dominating relaxation mechanism upon a reversal of the magnetic field direction is a physical rotation of the particle, known as Brownian relaxation. The characteristic frequency for Brownian relaxation dynamics is given by

$$f_B = \frac{k_B T}{6\pi\eta V_h}, \tag{1}$$

where $k_B T$ is the thermal energy, η is the dynamic viscosity and V_h is the hydrodynamic volume of the relaxing entity (e.g., a single MNP). The dynamic magnetic behavior can be described in term of the magnetic susceptibility χ with real (in-phase) and imaginary (out-of-phase) parts χ' and χ'', respectively. In case of a sinusoidal magnetic field $h_0 \sin(\omega t)$, the time dependent linear magnetic response can be expressed as

$$\chi(t) = M(t)/h_0 = \chi_0 \sin(\omega t - \theta) = \chi' \sin(\omega t) + \chi'' \cos(\omega t), \tag{2}$$

where $\chi' = \chi_0 \cos(\theta)$ and $\chi'' = \chi_0 \sin(\theta)$. At low frequencies the MNPs are able to rotate and follow the magnetic field, and the response is in-phase with the applied field. Therefore χ' is maximal. The rotation of the MNPs starts to lag behind the applied field at higher frequencies, which leads to a decrease in the in-phase component χ' and a corresponding increase in the out-of-phase component χ''. The out-of-phase component χ'' attains its maximum value at the Brownian relaxation frequency f_B.

A simple approach to account for a distribution of MNP sizes was introduced by Cole and Cole[1] according to the following expression for the complex magnetic susceptibility

$$\chi(\omega) - \chi_\infty = \frac{\chi_0 - \chi_\infty}{1 + (i\omega\tau_B)^{1-\alpha}}, \tag{3}$$

where α is the Cole-Cole parameter (ranging from 0 to 1, a measure of the nanoparticle size distribution width), $\tau_B = (f_B)^{-1}$ is the Brownian relaxation time, $\omega = 2\pi f$ is the angular frequency of the applied field and χ_0 and χ_∞ are the zero and high frequency limits of χ.

The dynamics is determined by the rotational behavior of the individual MNPs, which follows the Brownian relaxation dynamics. The modulation of the transmitted light is found in the complex second harmonic voltage output from the photodetector

$$V_2 = V_2' + \mathrm{i}V_2'', \tag{4}$$

where V_2' and V_2'' are the in-phase and out-of-phase signals, respectively. The modulation is measured using a lock-in amplifier with the AC magnetic field excitation as reference. From the perspective of transmitted light, the MNP ensemble will scatter light equally for a positive and negative magnetic field of the same amplitude. We therefore assume that the photodetector signal can be described as

$$V(t) = V_0 + V_{AC}\left|\sin(\omega t - \theta)\right| = V_0 + c\chi_0\left|\sin(\omega t - \theta)\right|, \tag{5}$$

where V_0 represents the un-modulated part of the transmitted light (used here for normalization), $V_{AC} = c\chi_0$ is the amplitude of the frequency dependent signal and c is a constant. The photodetector signal can further be expressed using the Fourier series for $|\sin(\omega t - \theta)|$, yielding

$$V(t) = V_0 + c\chi_0\left[\frac{2}{\pi} - \frac{4}{\pi}\left(\frac{1}{3}\cos(2\omega t - 2\theta) + \frac{1}{15}\cos(4\omega t - 4\theta) + \ldots\right)\right]. \quad (6)$$

Specifically, the second harmonic signal is given by

$$\begin{aligned} V_2(t) &= -\frac{4c\chi_0}{3\pi}\cos(2\omega t - 2\theta) \\ &= -\frac{4c\chi_0}{3\pi}\left(\cos(2\omega t)\cos(2\theta) + \sin(2\omega t)\sin(2\theta)\right) \\ &= -\frac{4c\chi_0}{3\pi}\left(\cos(2\omega t)\left(\cos^2(\theta) - \sin^2(\theta)\right) + 2\sin(2\omega t)\sin(\theta)\cos(\theta)\right) \\ &= -\frac{4c\chi_0}{3\pi}\left(\cos(2\omega t)\left((\tilde{\chi}')^2 - (\tilde{\chi}'')^2\right) + 2\sin(2\omega t)\tilde{\chi}''\tilde{\chi}'\right) \end{aligned} \quad (7)$$

,

where $\tilde{\chi}' = \chi'/\chi_0$ and $\tilde{\chi}'' = \chi''/\chi_0$. The lock-in detected in-phase and out-of-phase components of the second harmonic signal therefore become (rms values)

$$\begin{aligned} V_2' &= -2V_2(0)\tilde{\chi}''\tilde{\chi}' \\ V_2'' &= -V_2(0)\left((\tilde{\chi}')^2 - (\tilde{\chi}'')^2\right) \end{aligned} \quad (8)$$

where $V_2(0) = 4c\chi_0/3\sqrt{2}\pi$ is the zero frequency limit of V_2 (and V_2'').

The sign of V_{AC} depends on the optical scattering properties and the measurement geometry. For a geometry where the transmission is measured perpendicular to the axis of the applied magnetic field, as used in the present study, it is generally found that V_{AC} is negative for MNPs with sizes smaller than about 130 nm for blue laser light (λ = 405 nm). For even larger scattering entities, V_{AC} first becomes positive (e.g., for 250 nm MNPs) and then negative

(e.g., for 500 nm MNPs). This originates from the oscillation of the scattering cross-section with particle size as can be accounted for by Mie scattering theory.

In **Fig. S2a**, the normalized in-phase and out-of-phase components of the magnetic susceptibility, extracted from the Cole-Cole model, are plotted versus frequency. In **Fig. S2b**, normalized $\tilde{\chi}'\tilde{\chi}''$ and $(\tilde{\chi}')^2-(\tilde{\chi}'')^2$, have been plotted versus frequency to illustrate the shape of the two photodetector signals. The input susceptibilities, $\tilde{\chi}'$ and $\tilde{\chi}''$, are those displayed in **Fig. S2a**.

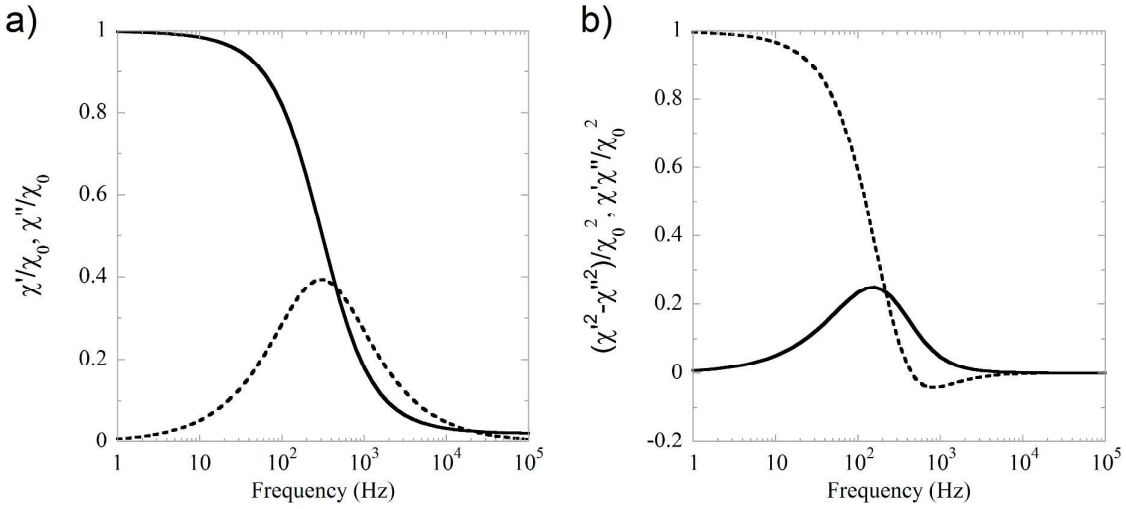

Figure S2. (a) Normalized susceptibility data (in-phase and out-of-phase represented by solid and dashed lines, respectively) extracted from the Cole-Cole model versus frequency (τ_B =300 s and α =0.15 were used as input). (b) Normalized $\tilde{\chi}'\tilde{\chi}''$ (solid line) and $(\tilde{\chi}')^2-(\tilde{\chi}'')^2$ (dashed line) versus frequency. The $\tilde{\chi}'\tilde{\chi}''$ curve represents the in-phase signal from the photodetector, whereas the $(\tilde{\chi}')^2-(\tilde{\chi}'')^2$ curve represents the out-of-phase signal from the photodetector.

Table S1. Sequences of target DNA (a conserved region of NDV strain Herts/33/NS fusion protein gene, GenBank accession number: AY117024), outer primers (F3/B3), inner primers (FIP/BIP) and loop primers (LF/LB).

Name	Sequence (5'→3')
Target DNA	TCTGACAAGCTCTCTTGATGGCAGGCCTCTTGCAGCTGCAGGGATCGTG GTAACAGGAGATAAAGCAGTCAACATATACACCTCATCCCAGACAGGG TCAATCATAGTCAAGTTACTCCCAAATATGCCCAAGGACAAAGAGGCG TGTGCAAAAGCCCCATTGGAGGCATACAACAGGACACTGACTACTTTG CTCACCCCCCTTGGTGATTCTATCCGCAGGATACAAG
F3	TGACAAGCTCTCTTGATGGC
B3	TGCGGATAGAATCACCAAGG
FIP	Biotin-ACCCTGTCTGGGATGAGGTGTATCTTGCAGCTGCAGGGAT
BIP	ATGCCCAAGGACAAAGAGGCGGGGGTGAGCAAAGTAGTCAG
LF	CTGCTTTATCTCCTGTTACCACG
LB	GCAAAAGCCCCATTGGAGGC

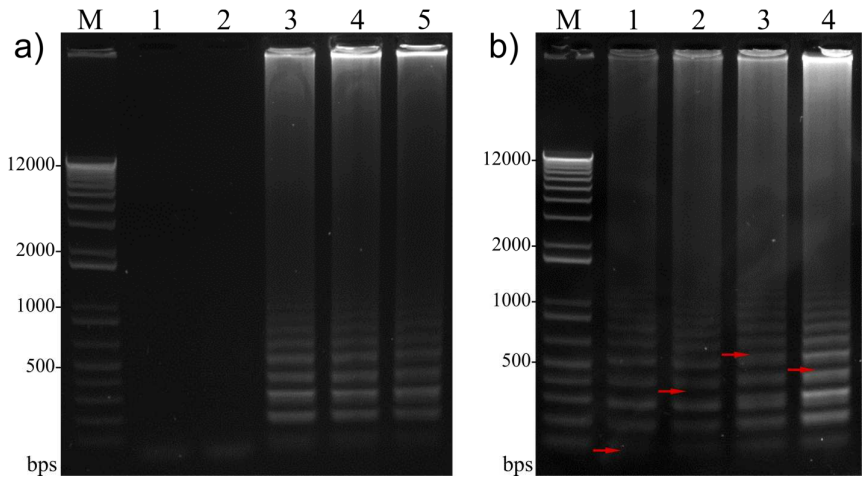

Figure S3. Agarose gel electrophoresis analysis results of LAMP reaction. (a) Temperature optimization; in lanes 1-5, the reaction temperatures are 61, 63, 65, 67 and 69 °C. (b) Primer optimization; in lanes 1-4, the concentrations of inner primers are 0.2, 0.4, 0.8 and 1.6 μM. Red arrows indicate the mean lengths of MNP-bound amplicons (MNPs at a final concentration of 100 μg/mL).

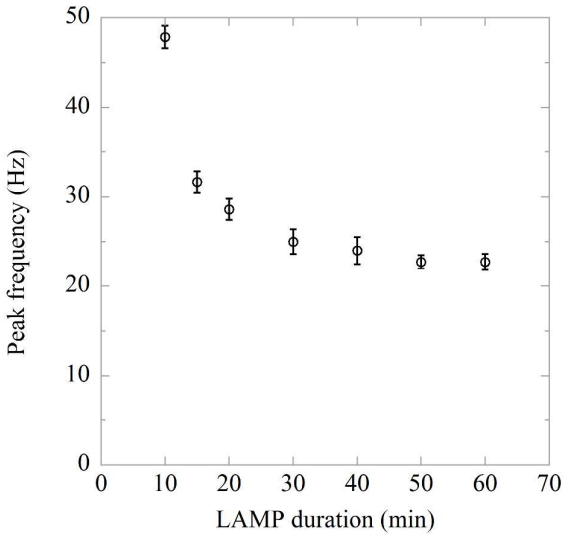

Figure S4. V_2'/V_0 peak frequency *vs.* LAMP duration for the detection of 1 pM synthetic target DNA. Error bars indicate one standard deviation based on three independent measurements.

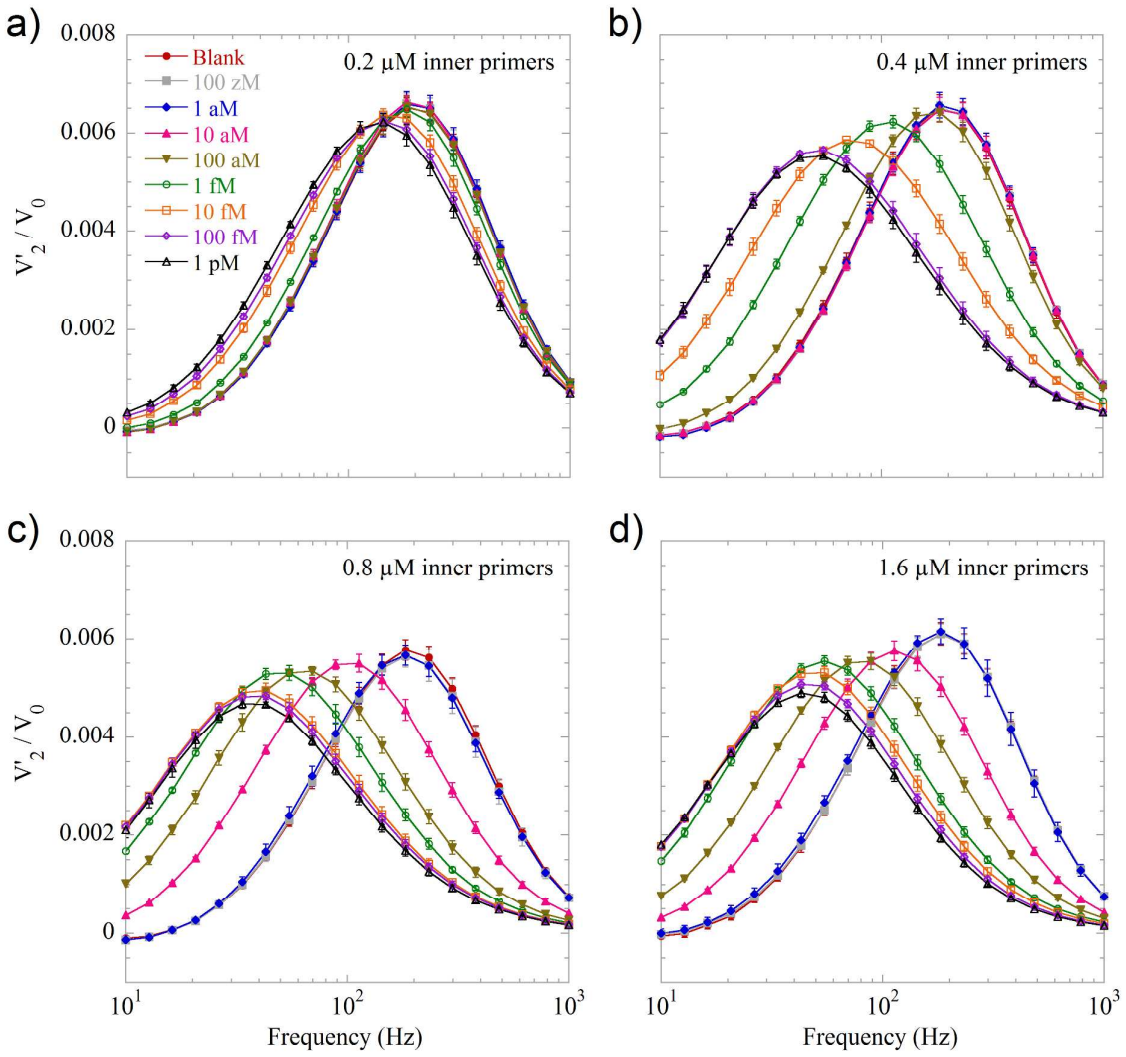

Figure S5. V_2'/V_0 spectra for the detection of indicated concentrations of synthetic DNA sequences using different inner primer concentrations, 0.2, 0.4, 0.8 and 1.6 μM in (a)-(d), respectively. (c) is identical to Figure 2a. Error bars indicate one standard deviation based on three independent measurements.

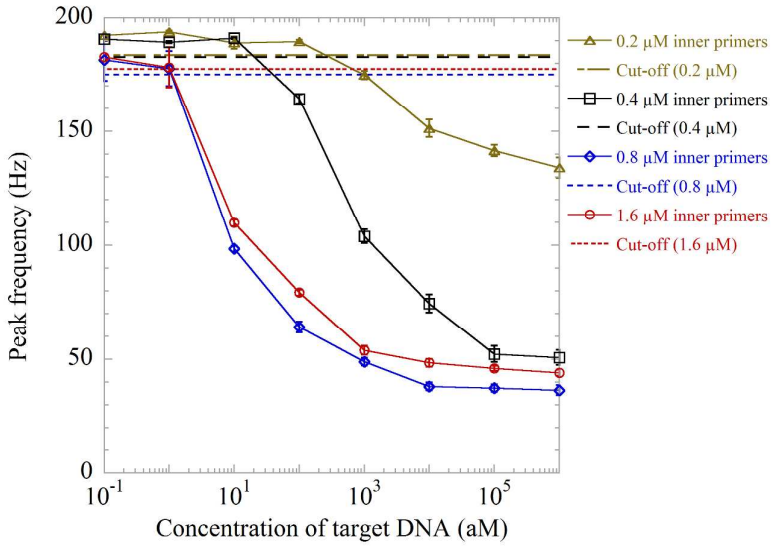

Figure S6. Peak frequency *vs.* target DNA concentration. Yellow triangles, black squares, blue diamonds and red circles represent inner primer concentrations of 0.2, 0.4, 0.8 and 1.6 μM, respectively. Error bars indicate one standard deviation based on three independent measurements. The cut-off values are indicated by the horizontal lines.

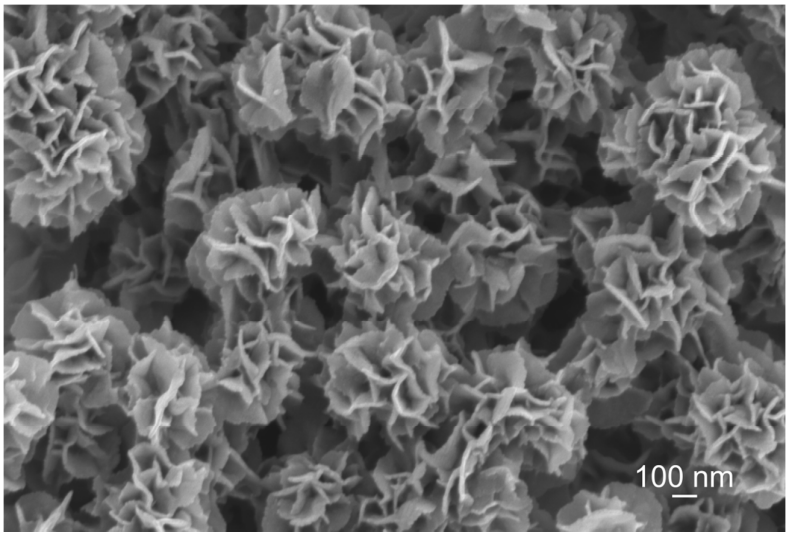

Figure S7. Scanning electron microscopy (Zeiss-1530) image of $Mg_2P_2O_7$ precipitation. The $Mg_2P_2O_7$ precipitation was collected by centrifugation after LAMP and washed twice by water.

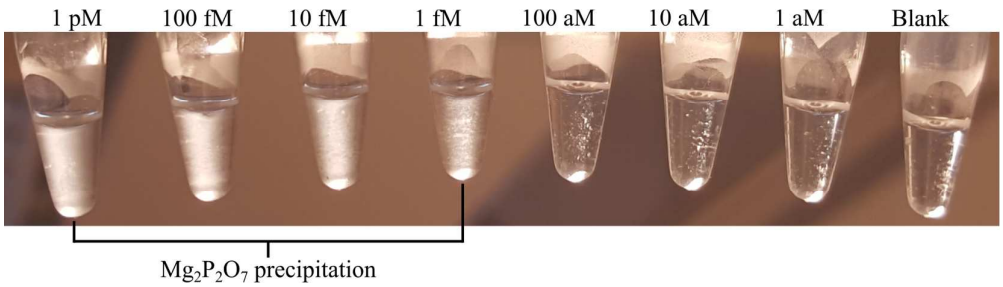

Figure S8. Sensitivity of visual inspection of LAMP products. Concentrations of the synthetic target DNA sequence are indicated. The concentration of inner primers is 1.6 μM, and the LOD of turbidity-based naked-eye judgment is 1 fM. The rightmost tube is a blank control sample.

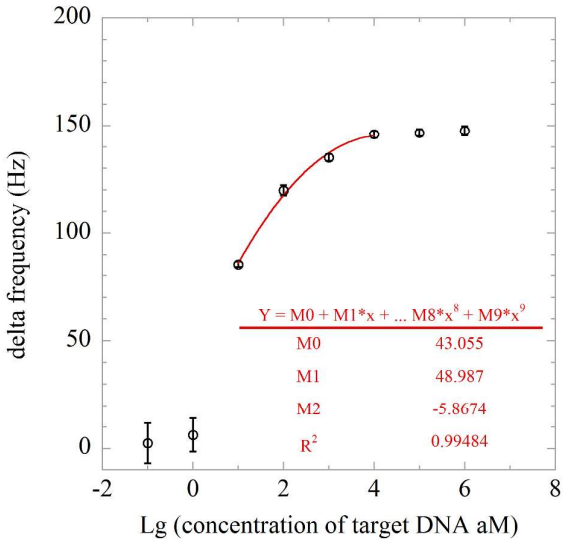

Figure S9. V_2'/V_0 peak frequency shift (with respect to the blank sample) *vs.* target DNA concentration. Error bars indicate one standard deviation based on three independent measurements. The trend line of dynamic detection range (10 aM to 10 fM) is indicated by the red curve.

REFERENCE

(1) Cole, K. S.; Cole, R. H. Dispersion and absorption in dielectrics I. Alternating current characteristics. *J. Chem. Phys.* **1941,** *9*, 341-351.